Bistatic Sensing with Reflected GPS Signals Observed With a Digital Beam-Steered Antenna Array

Kees Stolk and Alison Brown, NAVSYS Corporation

BIOGRAPHY

Kees Stolk is an engineer at NAVSYS Corporation working with simulation, design, and testing of NAVSYS advanced GPS systems including digital beam-steering, multipath estimation and reduction, and bistatic spatial signal processing. He has an MSc in Electrical Engineering from Twente University of Technology, Netherlands.

Alison Brown is the President and Chief Executive Officer of NAVSYS Corporation. She has a PhD in Mechanics, Aerospace, and Nuclear Engineering from UCLA, an MS in Aeronautics and Astronautics from MIT, and an MA in Engineering from Cambridge University. In 1986, she founded NAVSYS Corporation. Currently, she is a member of the USAF Scientific Advisory Board, a Member of the Interagency GPS Executive Board Independent Advisory Team (IGEB IAT), and an Editor of GPS World Magazine. She is an ION Fellow and was indoctrinated into the SBA "Wall-of-Fame" in 2003.

ABSTRACT

Reflected GPS signals have applications for remote sensing including: earth mapping, ocean surface mapping, terrain modeling and digital mapping through application of bistatic signal processing techniques. Previous research in such uses of reflected GPS has been limited by the weak signal power of these bistatic GPS signal returns. This paper describes the design of a Digital Beam-Steered antenna array, which is used to increase the Signal/Noise ratio of the GPS bistatic signal returns to allow sensing of both specular and diffuse GPS signals. Flight test data is presented to demonstrate the performance improvements possible using Digital-Beam-Steering for improved GPS bistatic signal processing and remote sensing.

INTRODUCTION

Early experimentation, using NAVSYS' advanced GPS receiver technology, demonstrated the ability to track the reflected GPS signals from the surface of the earth in the early 90s[1]. Since then, further research has demonstrated the utility of these signals for applications such as surface altimetry[2], wave motion detection and wind sensing[3], and observing surface water content[45] for mapping ice fields or wetlands.

Because of the extremely low power level of the returned bistatic GPS signals, this previous research has focused primarily on the strong specular bistatic signals. NAVSYS has developed a Digital-Beam-Steering GPS receiver, the High-gain Advanced GPS Receiver (HAGR), which can be used to increase the received signal/noise ratio from these weak bistatic signal returns allowing improved detection of both specular and diffuse GPS signals.

In this paper, the theoretical basis for GPS bistatic sensing is described, to describe the increased region of interest that can be leveraged for remote sensing by receiving both the GPS specular and diffuse signals. The design of the HAGR is presented and results are included from flight experiment showing the improved bistatic signal processing possible when using this Digital-Beam-Steering receiver as a remote sensing instrument.

DIFFUSE AND SPECULAR BISTATIC GPS SIGNALS

There are two types of bistatic GPS signals, diffuse and specular. Specular bistatic GPS signals are characterized by an optimal geometry, providing a very powerful reflection. Figure 1 shows the bistatic geometry and the specular points. The strength of the specular bistatic returns makes them easy to detect. The drawback,

however, is the limited area of the earth's surface they provide information on. The strength of the specular return depends on the smoothness of the surface. A smooth surface such as water provides much stronger specular returns than a rough surface such as forest.

Diffuse bistatic returns are produced by scattering of the GPS signal on the surface of the earth. Figure 1 shows that diffuse signal returns originate from a much larger area which could potentially provide information over a much larger region than possible by processing just the specular returns. However, these signals are extremely weak and require advanced receiver technology in order to be useful for remote sensing applications.

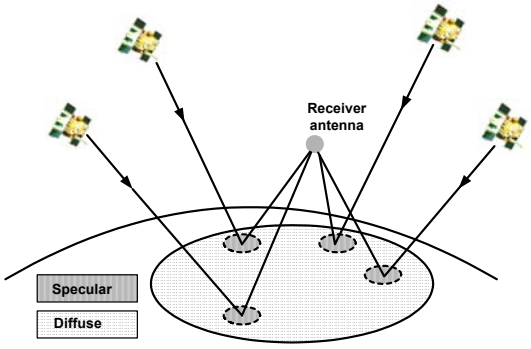

Figure 1 GPS Bistatic Geometry with Specular Reflection Points

RANGE/DOPPLER BISTATIC GPS SIGNAL PROCESSING

Figure 2 shows an example of a diffuse bistatic GPS scenario. The aircraft receives the direct signal from the satellite, traveling along the line of sight. The GPS bistatic antenna receives a diffuse reflection from the earth surface. For each point on the surface of the earth , the bistatic signal return is received with a range and Doppler offset relative to the aircraft. This information can be used to distinguish between bistatic signal returns from different points on the earth.

The doppler frequency of the bistatic signal relative to the direct signal, Δf (Hz), is computed as follows:

Equation 1

$$\Delta f_{\vec{x}} = \frac{\vec{v}_a \bullet \vec{k}_{\vec{x}} - \vec{v}_a \bullet \vec{k}_{sat}}{\lambda_{L1}}$$

Where

$\vec{v}_a$ aircraft speed (m/s)

$\vec{x}$ location where scattering occurs

$\vec{k}_{\vec{x}}$ line of sight from aircraft to scattering,

$\vec{k}_{sat}$ line of sight from aircraft to satellite

λ_{L1} GPS L1 wavelength (m)

The following expression describes the range of the bistatic return signal, $\Delta\tau$ (m), relative to the direct signal:

Equation 2

$$\Delta\tau = \left\|\vec{x}_a - \vec{x}\right\| + \left(\vec{x} - \vec{x}_a\right) \bullet \vec{k}_{sat}$$

Where

$\vec{x}_a$ location of aircraft

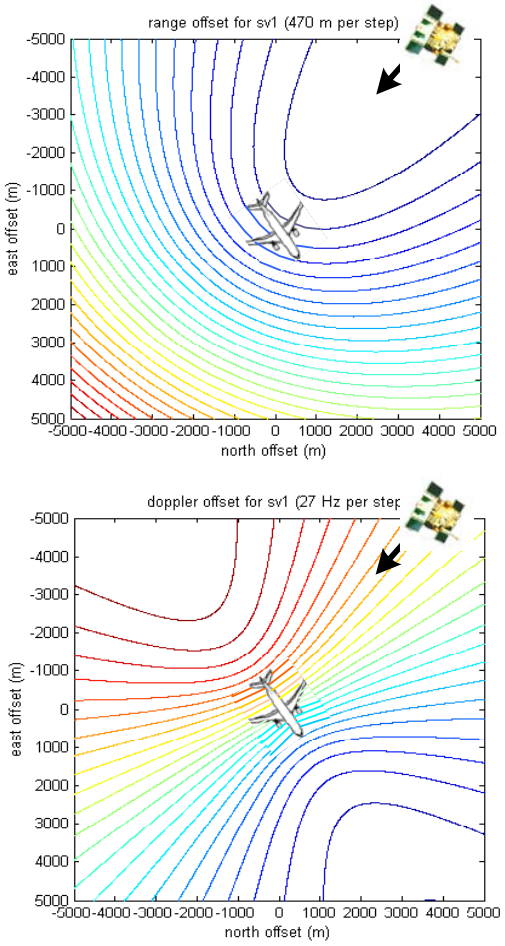

Figure 2 Equi-Range and Equi-Doppler Contours

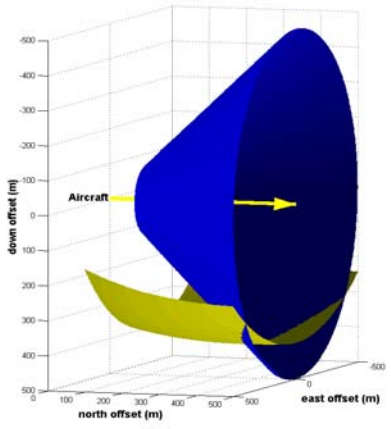

Figure 3 Diffuse Return Range/Doppler Ambiguity

It should be noted that a particular range/Doppler pair does not correspond to a unique 3-D point in space, but to a "slice" that can be represented by the intersection of the two surfaces shown in Figure 3. A constant Doppler region creates cone around the aircraft's speed vector, while constant range maps to an ellipsoid. The combination results in an ambiguity curve of possible locations from which range/Doppler bistatic return can come from. This ambiguity can be resolved if surface altitude is known. The HAGR Digital-Beam-Steering receiver also allows focusing of on a bistatic return from a certain location by the use of range selection, doppler selection and also beamsteering to assist in resolving this region of ambiguity.

BISTATIC SIGNAL/NOISE RATIO

In order to detect the weak GPS bistatic signal returns, advanced signal processing is needed to increase signal/noise ratio to an acceptable detection level. The amount a scatterer contributes to a bistatic return depends on the difference between selected range and doppler and those of the scatterer, and its distance to the beam center. This is captured in a mathematical expression:

Equation 3

$$SNR = \frac{C}{N_0} \cdot T \cdot \iiint_V F_C^2(\vec{x}) \cdot F_D^2(T, \vec{x}) \cdot F_B^2(\vec{x}) \cdot \frac{\sigma}{4\pi R^2} d\vec{x}$$

Where

C/N_0	carrier to noise power ratio (dBHz)
T	coherent integration time (s)
F_C	range filtering action
F_D	doppler filtering action
F_B	beam steering
σ	radar cross section coefficient (m^2/m^2)
R	range from plane to ground location (m)

The range filtering action depends on the geometry of the situation and the GPS code chip length. As shown in Figure 2 the area passed through the range filter forms a contour on the earth's surface. Equation 4 describes the range filter. Since this is a function of the chip length, there is a significant advantage to using the P(Y) code GPS signals for this processing which have 1/10th the chip length of the C/A code signals. The HAGR is able to track both the C/A and P(Y) code signals for approved users, and its reprogrammable architecture allows it to be upgraded for use with the future Civil signals which also will have smaller chip sizes than the 1.023 MHz C/A code. The new L5 civil code planned for the Block IIF GPS satellites will have a 10.23 MHz chip rate.

Equation 4

$$F_C(\vec{x}) = \max\left(1 - \frac{\left|\tau_{\vec{x}} - \tau_{\vec{x}_0}\right|}{L_{chip}}, 0\right)$$

Where

$\tau_{\vec{x}_0}$	range offset at focus point
$\tau_{\vec{x}}$	range offset at point scattering
L_{chip}	the chip length for the GPS code

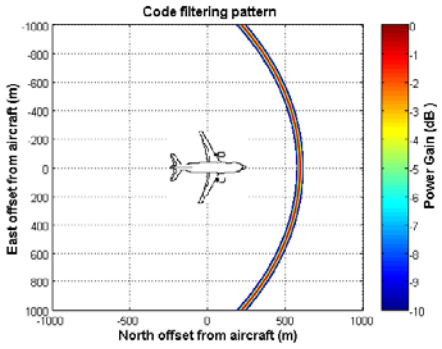

Figure 4 Range Filtering

The doppler filtering action passes an area shown by the curve in Figure 2. The width of this "strip" depends on the coherent integration time T (Equation 5). The coherent integration time is chosen to roughly match the range filter width.

Equation 5

$$F_D(T, \vec{x}) = \left|\mathrm{sinc}\left(f_{\vec{x}_0} T - f_{\vec{x}} T\right)\right|$$

Where

$f_{\vec{x}_0}$	doppler offset at focus point
$f_{\vec{x}}$	doppler offset at point of scattering

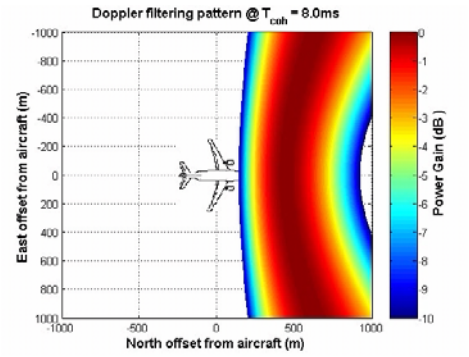

Figure 5 Doppler Filtering

The digital beam steering provides both gain and directional selectivity to resolve ambiguities. The signal gain depends on the number of elements (Equation 6). The HAGR can be configured with a variable number of antenna elements up to a total of 109-elements, as shown in Figure 6. For the first flight test a 15-element array was used, with the elements shown in red in Figure 6. Figure 7 and Figure 8 shows the 15-element and 109-element beam pattern created by this array. Through the HAGR digital control, these beams can be directed at any point on the surface of the earth for data collection. The area they cover is a function of the beam width and the aircraft altitude, as illustrated in Figure 9.

Equation 6

$$F_B\left(\vec{x}\right) = \frac{\left|\vec{e}_{\vec{x}_0}^{H}\vec{e}_{\vec{x}}\right|}{\sqrt{M}}$$

M number of antenna elements

$\vec{e}_{\vec{x}_0}$ steering vector at focal point

$\vec{e}_{\vec{x}}$ steering vector at point of interest

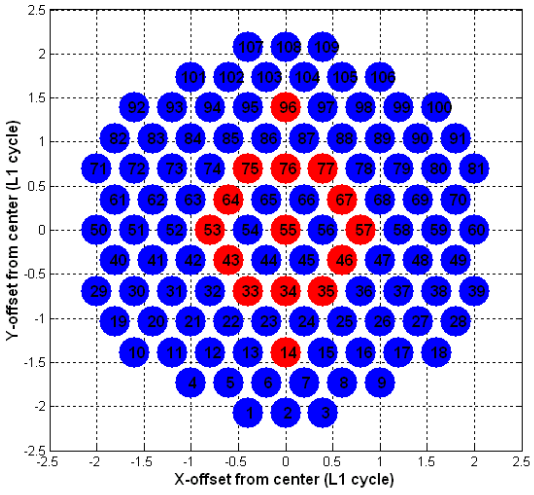

Figure 6 15 and 109 Element Phased Array

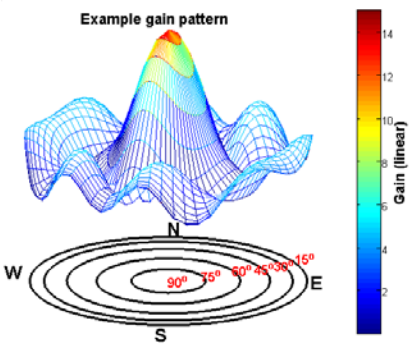

Figure 7 Beam pattern of 15 element phased array

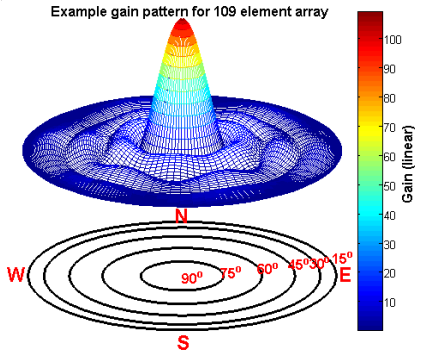

Figure 8 Beam pattern of 109 element array

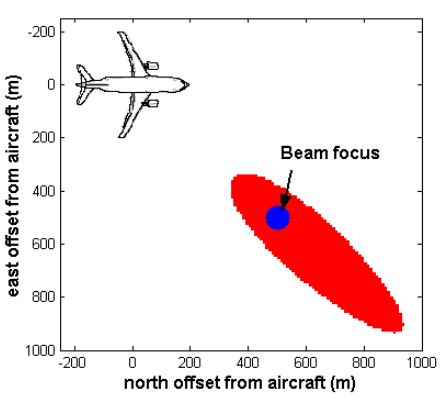

Figure 9 109 element Beam footprint (3dB contour from 500 m altitude)

DIGITAL BEAM-STEERING GPS RECEIVER

The NAVSYS High-gain Advanced GPS Receiver (HAGR) is a digital beam steering receiver designed for GPS satellite radio navigation and other spread spectrum applications. This is available for both military and commercial precision GPS applications and is installed in a rugged Compact PCI chassis which can be configured for either rack mount (Figure 10) or ATR (1½ LRU) installation for aircraft flight tests.

The HAGR system architecture is shown in Figure 11. The signal from each antenna element is first digitized

using a Digital Front-End (DFE). Each DFE card includes the capability to sample signals from 8 antenna inputs. These can be cascaded together to allow beam-steering to be performed from a larger antenna array. The complete set of DFE digital signals is then used to create the composite digital beam-steered signal input by applying a complex weight to combine the antenna array outputs. Up to 12 beams can be independently directed by the HAGR signal processing.

The HAGR can track up to 12 satellites simultaneously. In the normal mode of operation, the beams follow the satellites as they move across the sky (Figure 12). For bistatic signal processing, the beams can be directed at any particular point of interest on the earth. The array weights are applied independently for each of the HAGR signal processing channels which allows the antenna array pattern to be pointed in any direction through software control.

Figure 10 HAGR Assembly

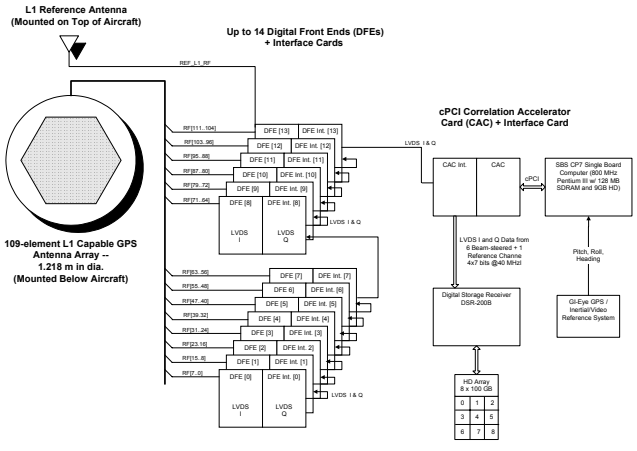

Figure 11 HAGR System Architecture

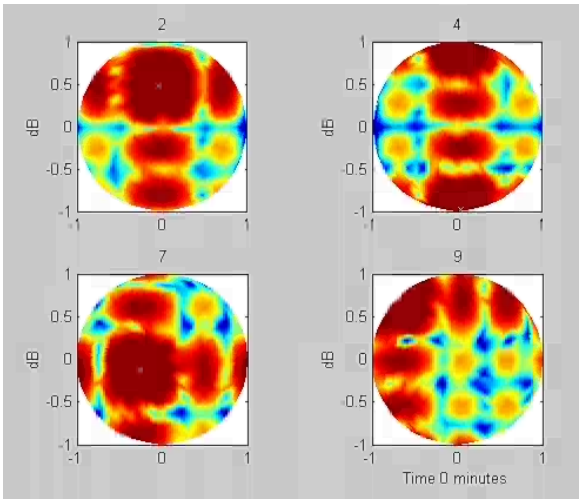

Figure 12 Satellite Beam Steering Mode

BISTATIC GPS FLIGHT TEST

The first flight test was conducted with the 15-element Digital-Beam-Steering GPS Bistatic sensing system shown in Figure 13. This was installed on the under-side of a Cessna test aircraft and a reference antenna was installed on the upper-side of the aircraft. During this flight test, the HAGR was used to track the GPS satellites and the raw broad-band data was also recorded from each of these elements, and a reference antenna using our Advanced GPS Hybrid Simulation (AGHS) digital storage capability[67]. Approximately one hour of bistatic maritime data and two hours of bistatic land data was collected. Using the AGHS, this was then played back into the HAGR for signal processing post-test.

Figure 13 Cessna Test Aircraft and Antenna Array Mounted underneath

To instrument the test, we also installed in the aircraft our GI-Eye GPS/inertial/video georegistration system[89]. This recorded the scenes from below the aircraft for use as a truth reference. The precision georegistration capability of this system also allowed targets of opportunities to be precisely gelocated within the imagery for use in post-test analysis of their corresponding bistatic GPS signatures. Figure 14 shows the view from under the aircraft of come of the land and ocean data collected from the GI-Eye during this flight test.

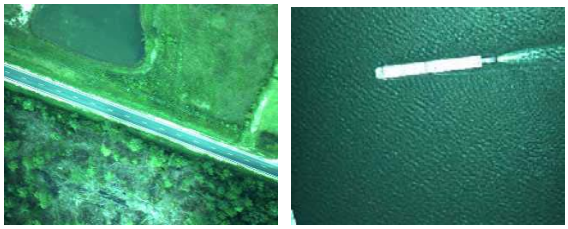

Figure 14 Land and Maritime surface

SPECULAR DATA ANALYSIS

Analysis of the specular return over land can be used to provide information on both elevation[2] and also the land-type where the signal is being returned (e.g. water content)[4,5]. For example, Figure 15 shows a dramatic increase in return power when the specular point crosses the Pearl River in a forest on the Mississippi-Louisiana border. The rough surface formed by the treetops provides a low specular return whereas the smooth river surface provides a very strong return.

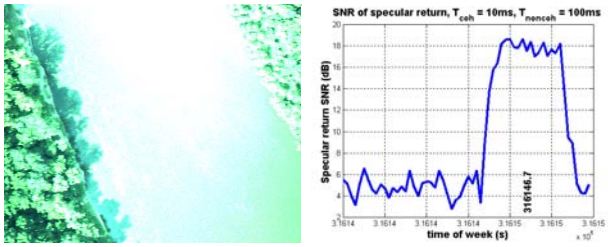

Figure 15 Pearl River crossing, specular power increase

MARITIME DIFFUSE DATA ANALYSIS

Over water, there is a very strong specular return and a very weak diffuse signal return. To bistatic GPS data was analyzed over water to determine whether it could be used to detect signals of interest from the diffuse bistatic signal returns from vessels on the surface of the water. The recorded GPS data was analyzed over a surface area containing the stationary oil tanker shown in Figure 17. As shown in Figure 17, this target was at some distance from the specular regions of the GPS signal returns. The post-processed bistatic signal returns from the satellite signals processed are shown in scenario. The results shown in Figure 18 indicate a strong return from the tanker's location only from one of the satellite signal, SV 14 only. From examination of Figure 17, this was the only satellite signal that provided a bistatic backscattered return. This indicates, that this target was likely detected from back-scatterred GPS signals returned through a corner reflection type of effect.

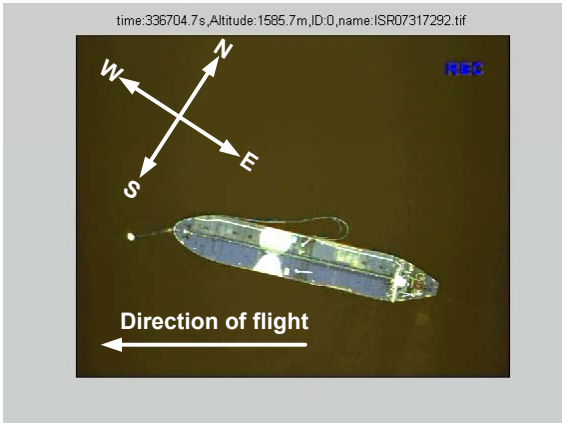

Figure 16 Direction of Flight

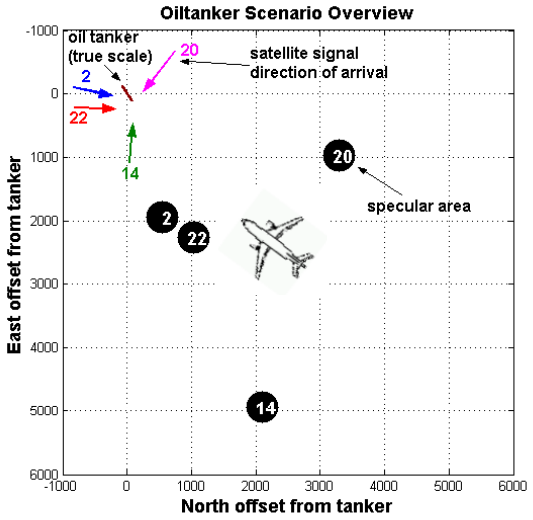

Figure 17 Maritime bistatic scenario

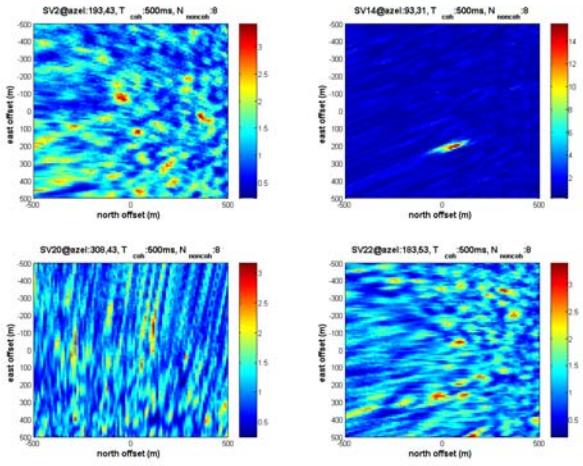

Figure 18 Maritime Bistatic Diffuse Signal Returns (Strong return only for satellite 14)

LAND DIFFUSE DATA ANALYSIS

The recorded data was also analyzed to evaluate the magnitude of the diffuse bistatic GPS returns over land. This data was also used to build a GPS bistatic signal simulation tool for use in predicting the magnitude of the bistatic signatures as a function of the signal geometry and the modeled land clutter coefficients For our analysis, we selected the following geometry of interest. (Figure 19) :

- receiver grazing angle > 30º (limits the range to the diffuse reflection point)
- transmitter grazing angle > 30º (limits satellite selection to higher satellite elevations)
- angle between bistatic bisector and up axis < 30º (selects region surrounding the specular point).

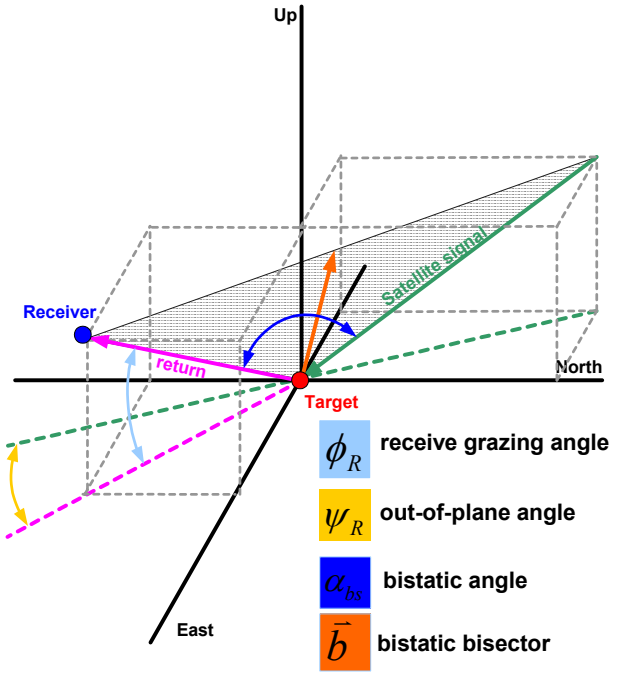

Figure 19 Bistatic geometry descriptors

Figure 20 shows how these constraints map to ground surface. The line in the figure connects locations where equi-range and equi-doppler curves run parallel. These locations are expected to produce strong returns. Figure 21 shows how these constraints map to a bistatic range and doppler surface. Locations with strong returns are expected on the edge of this range/doppler surface.

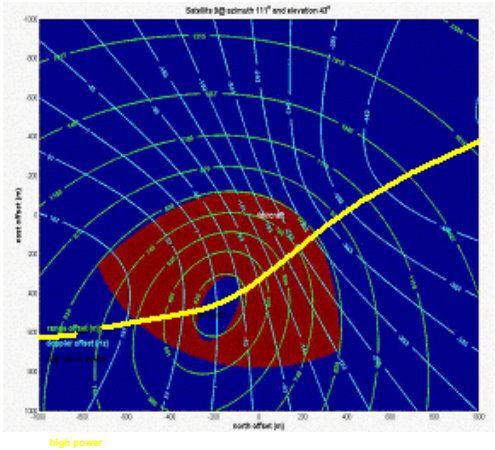

Figure 20 Analyzed ground surface area

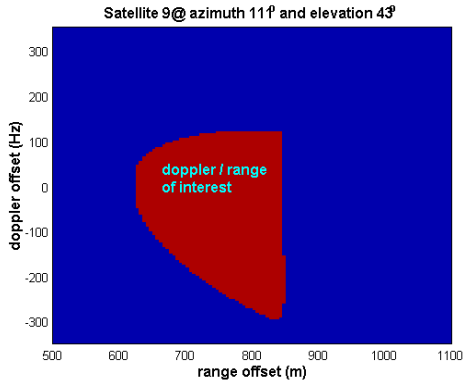

Figure 21 Range/Doppler surface of interest

The bistatic signal returns from this region of interest were analyzed to compare the received signal levels against a simulation tool developed by NAVSYS in Matlab to model the strength of the bistatic return over a surface area. Figure 22 to Figure 27 compare the results of the model-based simulation and the actual processed bistatic signal returns from the flight test data. This shows that we have good correspondence between the bistatic simulation model and the real-world data. Because of the low level of the signal returns, reliable bistatic signal detection is only possible with the 15-element array over the region encompassing the range/doppler boundary which maps to the yellow line in Figure 20. This is the region where the range/Doppler contours are nearly parallel increasing the surface area for a single code/Doppler integration cell (see Equation 3).

The Matlab model-based simulation tool was used to predict the area of coverage over which bistatic GPS signals could be expected to be detected for the 109 element antenna array which will be used in the next scheduled flight test. From Figure 28, this predicts that a much larger region of interest is covered using this larger version of the phased array which will open up some interesting new opportunities for remote sensing applications.

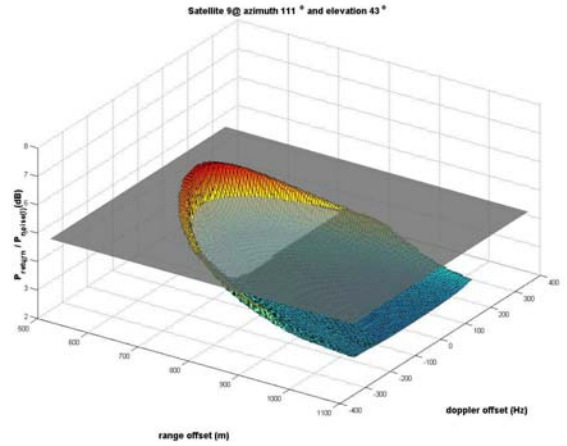

Figure 22 Modeled Bistatic Signals SV 9 (SNR Peak=7 dB)

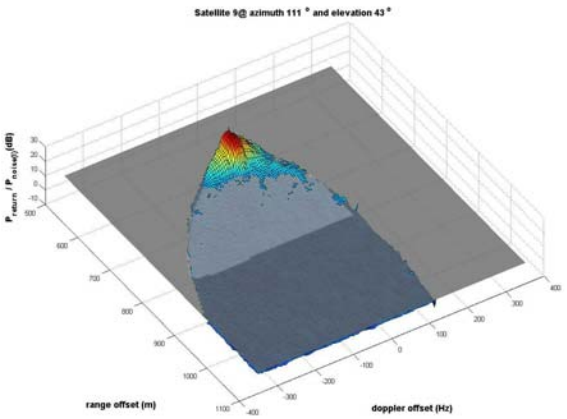

Figure 23 Actual Bistatic Signals SV 9 (SNR Peak=24 dB)

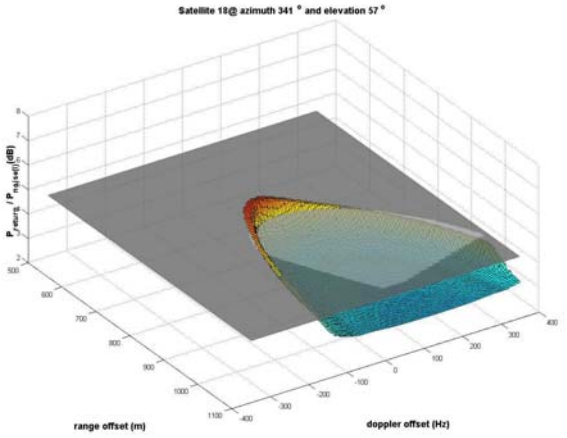

Figure 24 Modeled Bistatic Signals SV 18 (SNR Peak=6.5 dB)

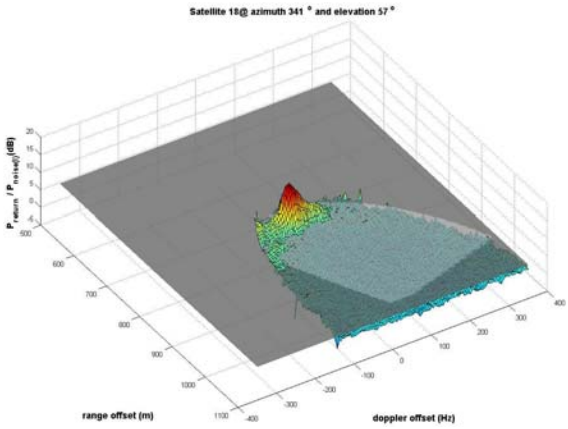

Figure 25 Actual Bistatic Signals SV 18 (SNR Peak=14 dB)

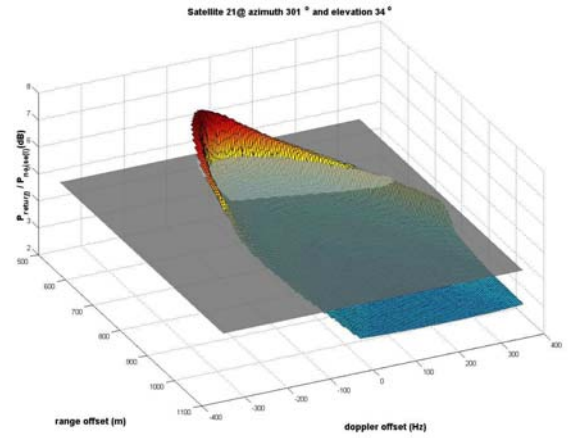

Figure 26 Modeled Bistatic Signals SV 21 (SNR Peak=7 dB)

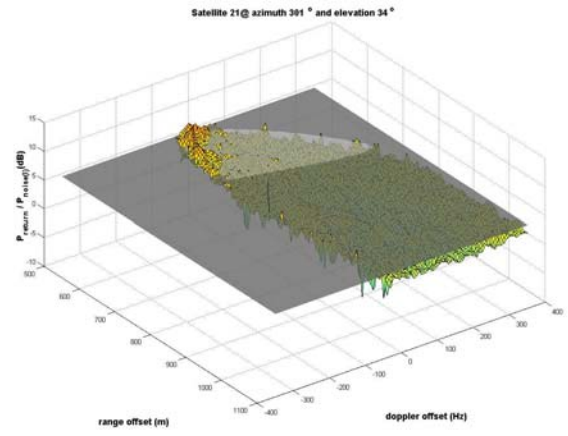

Figure 27 Actual Bistatic Signals SV 21 (SNR Peak=7.5 dB)

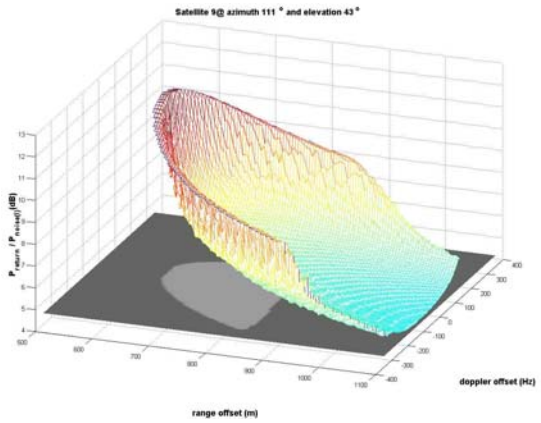

Figure 28 Simulation for 109 element array (SV 9)

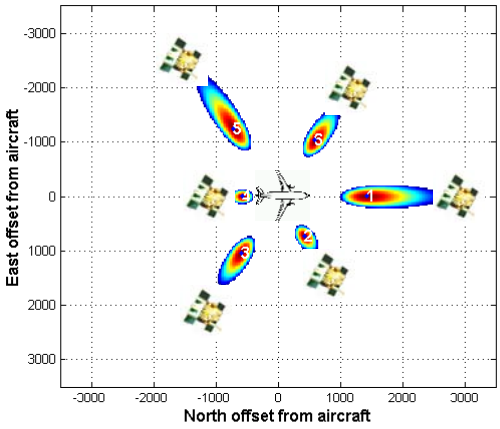

Figure 29 3dB Footprints Towards Specular Point at 500 m Altitude

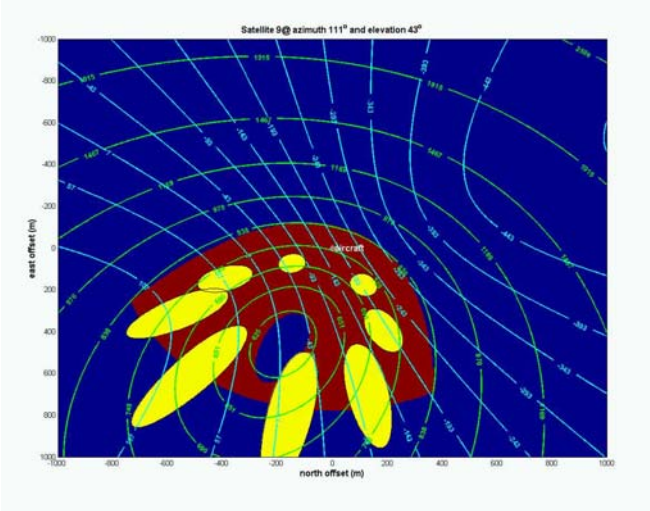

Figure 30 3dB Footprint Pattern for Diffuse Bistatic Signals

CONCLUSION

The test results and analysis described in this paper has demonstrated the ability of the HAGR receiver to improve the GPS bistatic remote sensing capability by using a Digital-Beam-Steered to allow weak GPS signal returns to be detected. The flight test results collected using a 15-element Digital-Beam-Steered phased array were used to demonstrate the following performance improvements possible with this receiver design.

- Robust detection and tracking of specular signals over both land and water
- Detection of diffuse signal returns over water from some surface vessels where backscatter occurred
- Detection of diffuse signal returns over a region of interest over land

We are currently in the process of assembling a 109 element phased array for the next flight test. This will provide the ability to boost the received bistatic signal returns by +20 dB gain using 10 software controlled beams. We plan to collect more test data during this flight using these beam directed to both the specular return points (see Figure 29) and covering the diffuse region of interest (see Figure 30). This +20 dB beam-steering capability is expected to further improve GPS bistatic signal analysis both by increasing the signal gain and also by removing range/Doppler ambiguity effects from the signal returns through the small beam-footprint.

ACKNOWLEDGEMENTS

The authors would like to acknowledge the support of Charles Luther of Office of Naval Research for sponsoring this activity. This work was funded under SBIR Contract No. N00014-00-C-0552.

REFERENCES

[1] J. Auber at al, "Characterization of Multipath on Land and Sea at GPS Frequencies", Proceedings of the Institute of Navigation GPS-94 Conference, Salt Lake City, Utah

[2] Masters, D., P. Axelrad, V. Zavorotny, S.J. Katzberg, and F. Lalezari, "A Passive GPS Bistatic Radar Altimeter for Aircraft Navigation," *ION GPS-2001*, Salt Lake City, OR, p. 2435-2445, September 2001

[3]Zavorotny, V.U., "Bistatic GPS Signal Scattering from an Ocean Surface: Theoretical Modeling and Wind Speed Retrieval from Aircraft Measurements," Workshop on Meteorological and Oceanographic Applications of GNSS Surface Reflections: from Modeling to User Requirements, July 6, 1999, De Bilt, The Netherlands, http://www.etl.noaa.gov/~vzavorotny/

[4] J. Garrison, S. Katzberg, "The application of reflected GPS signals to ocean and wetland remote sensing," In the Proceedings of the Fifth International Conference on Remote Sensing for Marine and Coastal Environments, San Diego, CA, 5-7 October, Vol. 1, pp. 522-529, 1998.

[5] Masters, D, et al, "GPS Signal Scattering from Land for Moisture Content Determination", http://www-ccar.colorado.edu/~dmr/doc/pubs/files/igarss_soil_final.pdf

[6] A. Brown and N. Gerein, "Advanced GPS Hybrid Simulator Architecture", Proceedings of ION 57th Annual Meeting 2001, Albuquerque, NM, June 2001

[7] http://www.navsys.com/Products/aghs.htm

[8] D. Sullivan and A. Brown, "High Accuracy Autonomous Image Georeferencing Using a GPS/Inertial-Aided Digital Imaging System", Proceedings of ION National Technical Meeting 2002, San Diego, CA, Jan. 2002

[9] http://www.navsys.com/datasheets/NAVSYS_Gi-Eye.pdf